Deciphering the Role of Noncovalent Interactions in the Conformations of Dibenzo-1,5-dichalcogenocines

Robin Weiss, Yann Cornaton, Hassan Khartabil, Loïc Groslambert, Eric Hénon, Patrick Pale, Jean-Pierre Djukic, Victor Mamane

Deciphering the Role of Noncovalent Interactions in the Conformations of Dibenzo-1,5-dichalcogenocines

Robin Weiss,[a] Yann Cornaton,[b] Hassan Khartabil,[c] Loïc Groslambert,[a,b] Eric Hénon,[c] Patrick Pale,[a] Jean-Pierre Djukic*[b] and Victor Mamane*[a]

Dedication ((optional))

[a] Dr. R. Weiss, Loïc Groslambert, Prof. Dr. P. Pale, Dr. V. Mamane
Institute of Chemistry of Strasbourg, UMR 7177 - LASYROC
CNRS and Strasbourg University
4 rue Blaise Pascal, 67000 Strasbourg, France
E-mail: vmamane@unistra.fr (VM)
[b] Dr. Y. Cornaton, Dr. J.-P. Djukic
Institute of Chemistry of Strasbourg, UMR 7177 - LCSOM
CNRS and Strasbourg University
4 rue Blaise Pascal, 67000 Strasbourg, France
E-mail: djukic@unistra.fr (JPD)
[c] Dr. H. Khartabil, Prof. Dr. E. Hénon
CNRS, ICMR UMR 7312
Université de Reims Champagne Ardenne
51097 Reims, France

Supporting information for this article is given via a link at the end of the document.((Please delete this text if not appropriate))

Abstract: A combined experimental and theoretical study is reported on the new dibenzo-1,5-ditellurocine **2-Te** in order to get an overview on the parameters controlling conformational change and to explain the differences with sulfur and selenium analogues. The boat to chair conformer preference is revealed by DFT calculations. For **2-Te**, a ΔG value of about 3 kJ/mol was calculated, close to the value measured by NMR (5 kJ/mol). However, DFT calculations with implicit solvation effects could not clearly establish the presence of an intramolecular Te---HC noncovalent interaction (NCI), as observed in the solid state. The Independent Gradient Model (IGM) methodology discloses an existent but probably not sufficiently discriminating Te---HC NCI. It also confirms that van der Waals interactions between phenyl rings is a source of stabilization of the boat conformer. Furthermore, electrostatic potential analysis suggests that chalcogen bonds between Te σ-holes and solvent might play an important role.

Introduction

Conformational changes are ubiquitous in many chemical and biological processes.[1,2] (Macro)cyclic molecules and macromolecular species, natural or not, such as macrolides, proteins, nucleic acids, etc, usually adopt various conformations, that evolve upon external stimuli, such as ligand binding, light, chemical transformation or modification of their environment. Although this phenomenon is increasingly exploited in switchable materials[3] or molecules,[4] in drug design, as for riboswitches,[5] foldamers,[6] and in sensing,[7] the basic understanding is not always established, especially when conformational changes are due to noncovalent interactions (NCIs). The latter can be present either when establishing contact between stimulus and stimuli-responsive entities or within the responsive molecule, both leading to conformational preference. Thus, understanding how NCIs participate in the specific stabilization of one conformer over the others is a prerequisite toward their utilization in the control of dynamic processes.

In the latter context, dibenzocyclooctadienes **1** and their heterocyclic derivatives could serve as models due to their flexible nature and their so-induced interesting conformational changes. They indeed exhibit two main stable conformations, namely chair (**C**) and boat (**B**) conformations (Figure 1).[8] Conformation **B** is usually predominant in solution, while **C** is always observed in the solid state of compounds whose X-ray structures are available.[9] For charged molecules, the **C** conformer becomes predominant and even almost exclusive also in solution, probably because of repulsive coulombic interactions.[9d,10]

Surprisingly, the key factors that guide the conformational preference of these derivatives were studied in rare cases. Lu and co-workers recently demonstrated that substitution of the benzene rings of dibenzocyclooctadienes **1** influenced the **B/C** equilibrium: intramolecular hydrogen bond (HB) between the substituents stabilizes **1B** whereas electron repulsive interactions favors **1C**.[11] Interestingly, the **B/C** interchange temperature could be raised from -60 to 60°C by finely tuning the position and NCI properties of the substituents. More recently, Ishiwari and co-workers showed that 1,5-diaza analogues adopt straight-shape twisted conformation with a transannular NH HB, but change to more or less bent boat-type structures upon mono- or di-protonation.[12]

The involvement of a putative intramolecular HB was also reported between Se and H of the methylene groups in the selenated analog of **1**, namely dibenzo-1,5-selenocine **2-Se**[13] (Figure 1). In this work, the authors noticed shorter distances in (calculated) **2-SeB** than in **2-SeC**, which “may indicate a stronger C-H---Se nonbonded interaction in **2-SeB** than in **2-SeC**”. At equilibrium in solution ($CDCl_3$, -22°C), the boat conformation is preferred with a **B:C** ratio of 83:17, similar to the ratio observed in

the case of 1,5-dithiocine **2-S** at lower temperature (80:20 in $CDCl_3$–CS_2 1:1 at -66°C).[8a]

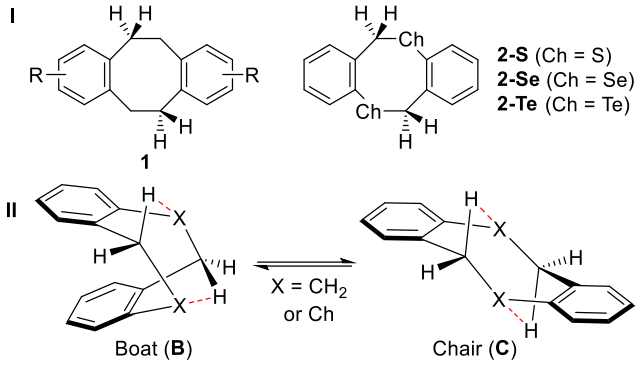

Figure 1. (I) Dibenzocyclooctadienes (**1**) and dibenzodichalcogenocine analogs (**2**); (II) Conformational equilibrium in solution (red dashed lines denotes the possible Ch---H interaction).

With the aim to study the role NCIs may have in the higher stability of the **B** conformation in dichalcogenocines **2**, we report herein the first synthesis of dibenzo-1,5-ditellurocine **2-Te** and its experimental and theoretical conformational analysis (Figure 1). Considering the special nature of tellurium in the chalcogen series,[14] we wondered if substitution of sulfur or selenium by tellurium atoms in compounds **2** could modify the intra- and inter-molecular NCIs and cause variations in the **B/C** equilibrium temperature, with potential applications based on shape-changing structures.[2] In regard to the highlighted Se---H interaction in **2-Se**,[13] an open question was to see if whether or not an analogous Te---H interaction[15] could be observed in **2-Te**. It is worth noting that most of Te---H NCIs were observed in the solid state[16,17] and only one recent example reported its study in solution in peculiar silatellurone derived from bis(diazasilete).[18] However, in this case, the Te=Si double bond is polarized with an important $Si^{\delta+}$–$Te^{\delta-}$ character that facilitates the Te---H interaction.

In addition to the study of the conformational potential energy surface of these systems (minima, transition states), a special focus has been placed on the accurate characterization of intramolecular NCIs. In previous studies reported on dibenzocyclooctadiene derivatives,[9a,9c,11,13] transannular interactions were assessed by means of different theoretical strategies ranging from the simple examination of molecular models or bond distance measurement, to the calculation of van der Waals potential[19] and of electron density maps. But, to our knowledge, no attempt of direct quantification of these intramolecular interactions has so far been performed on these systems. In the present paper, from a modern electron-density-based method, we aim at carefully identifying and quantifying those interactions, possibly responsible for conformational preference in isolated molecules. Sophisticated methods for the accurate description of NCIs exist like SAPT[20] or variational energy decomposition schemes,[21] with recent intramolecular schemes.[22] In other respects, the IQA[23] technique is a remarkable approach to perform quantitative studies of all kind of interactions. Unfortunately, it is very time-consuming, limiting its application to small systems. Here, we employ the relatively recent Independent Gradient Model (IGM) methodology.[24] This cheaper tool is particularly attractive to capture and characterize NCIs that occur in an intramolecular fashion between atoms or sub fragments in one single molecule (for instance to characterize intramolecular π-π stacking or HB).

Results and Discussion

Synthesis

With the aim to disclose a short and efficient synthesis of **2-Te**, the [4+4] dimerization of the quinoid form (**3-Q**) of benzotellurete **3** was envisaged in analogy to benzothietes[25] and benzoselenetes.[26] Although not yet described nor detected as an intermediate, benzotellurete **3** was predicted to be more stable than its sulfur and selenium analogues.[27] Tellurolates **4** were identified as possible intermediates for the formation of **3** either directly by intramolecular S_N2 reaction (red path) or indirectly through MX elimination (blue path) (Figure 2).

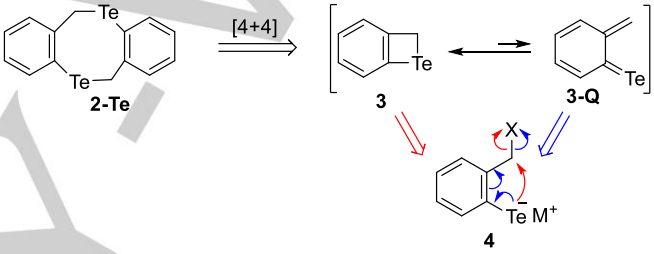

Figure 2. Envisaged synthesis of ditellurocine **2-Te**

Thus, *ortho*-chloro- or fluoromethylphenyl iodides (**5a**-**b**) were reacted with *t*-BuLi at -78°C followed by addition of grey tellurium and temperature raising to generate lithium tellurolates **Li-4a** and **Li-4b**, respectively (Scheme 1). Their formation was evaluated by analyzing the mixture obtained after quenching the reaction with ethanol at different temperatures (-70°C, -40°C and 0°C) followed by air oxidation. Under these conditions, the amount of isolated ditellurides **6a** and **6b** would give a good picture of the amount of tellurolates **Li-4a** and **Li-4b** present in the reaction mixture at a given temperature. No ditelluride **6a-b** was detected at -70°C indicating that this temperature is too low to permit tellurium insertion. At -40°C, only ditelluride **6b** could be isolated with a high yield of 91%. It is probable that in the case of **5a**, the lithio derivative decomposed while raising the temperature before tellurolate **Li-4a** could be generated. In contrast, tellurolate **Li-4b** was cleanly generated from **5b** at a temperature comprised between -70 and -40°C. Pleasingly, at 0°C, 1,5-ditellurocine **2-Te** was obtained with 72% yield from **5b**. This result suggests that, between -40 and 0°C, tellurolate **Li-4b** evolved to benzotellurete **3** (Figure 2) which in situ dimerized to ditellurocine **2-Te**, probably through the quinoid intermediate **3-Q** whose formation should increase with temperature. As **2-Te** might also be produced through a bimolecular double S_N2 mechanism from **Li-4b**, a test reaction involving lithium phenyltellurolate and compound **7** was attempted to check the validity of such mechanism (Scheme 1, bottom). Under similar conditions, no coupling product **8** could be detected upon raising the temperature from -78°C to 0°C, and

compound **7** was completely recovered. The formation of **2-Te** thus proceeds through the quinoid intermediate **3-Q**.

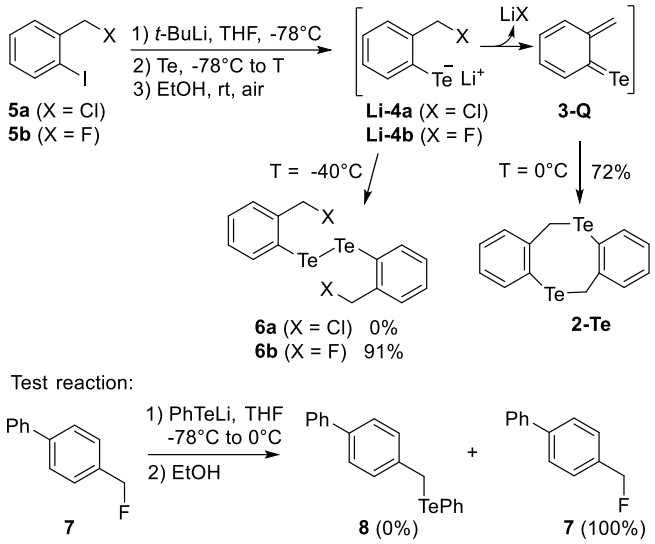

Scheme 1. Attempts for the synthesis of ditellurocine **2-Te** from iodoaryles **5a,b**.

X-Ray Analysis

The solid-state molecular structure of ditellurocine **2-Te** was determined by single-crystal X-ray diffraction (Figure 3). In sharp contrast to diselenocine **2-Se** and other dibenzocyclooctadiene analogues, ditellurocine **2-Te** adopts the **B** conformation in the solid-state. A close Te---H contact is observed between Te atom and the endocyclic hydrogen with a distance of 2.838(8) Å, well below the sum of van der Waals radii (r_{vdwTe} = 2.08 Å, r_{vdwH} = 1.20 Å) (Figure 3, left). Moreover, the molecular packing of **2-Te** is dominated by intermolecular Te---Te contacts (green lines, *d*(Te-Te) = 3.724(8) Å, *θ*(C-Te-Te) = 166.5°) leading to a distorted Te_4 square (Figure 3, right). Additional CH---π contacts (red dashed lines) may participate to the overall stabilization of the molecular packing. The geometrical parameters of Te---Te contact suggest that intermolecular chalcogen bonds are key interactions in the molecular packing of ditellurocine **2-Te**.[28] This particular point will be discussed in the last section through electrostatic potential analysis.

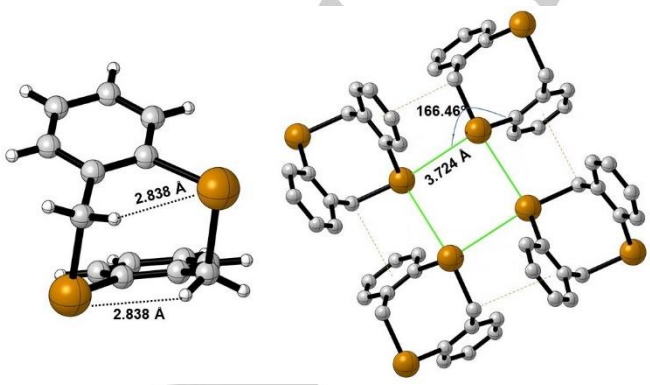

Figure 3. Left: X-ray structure of ditellurocin **2-Te** using CYLView.[29] Right: view of the crystal packing revealing intermolecular short distances; hydrogen atoms are omitted for clarity. Color code: carbon in grey, hydrogen in white and tellurium in orange.

Conformational analysis by DFT calculations

To better understand the flexibility of the tellurocine **2-Te** and look for Te---H bond, the conformational equilibrium of tellurocine **2-Te** was theoretically investigated by DFT-D4 methods, taking implicit solvation effects of $CHCl_3$ and CH_2Cl_2 into account with the COSMO continuum screening model. As was previously observed for dibenzocyclooctadiene **1** and its analogs,[8,9,13] three conformers have been characterized as local energy minima, a chair-like (**C**) conformer, a boat-like (**B**) conformer and a twisted (**T**) one (Figure 4). The three conformational transition states have also been optimized, **[TS1]**‡ being the transition state for the **B**→**C** transformation, **[TS2]**‡ for **B**→**T**, and **[TS3]**‡ for **C**→**T**.

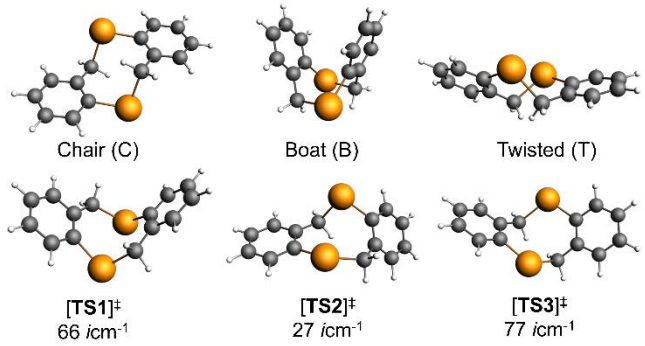

Figure 4. 3D singlet state structures of the three stable conformers of **2-Te** and the conformational transition states between them computed at the COSMO($CHCl_3$)-ZORA-PBE-D4(EEQ)/all electron TZP level. Similar geometries were computed with COSMO(CH_2Cl_2) (see S. I.).

The main conformational difference between tellurocine **2-Te** and dibenzocyclooctadiene **1** is about the "boat" conformer. While for **1,** the actual "boat" conformer (*i.e.* parallel C_{sp3}-C_{sp3} bonds) is a transition state between two degenerate stable "twisted boat" conformers,[8d-e] only one conformer of tellurocine **2-Te** has been found to be a local energy minimum in the "boat" region (see Figure S12 in S. I.). All tentative optimizations of a "twisted boat"-like conformer eventually led to the actual "boat" conformer. This difference can be attributed to the symmetry breaking induced by the replacement of a CH_2 fragment by a Te atom, the two "twisted boat" conformers thus become inequivalent. In the case of **2-Te**, the local energy minimum is found to correspond to an actual (parallel C_{sp3}-C_{sp3} bonds) "boat" conformation. The same behaviour can be observed for the other chacolgenocines **2-S** and **2-Se** (see Figure S12 in S. I.).

As already established for dibenzocyclooctadiene **1**,[8] each of the three stable conformers (**C**, **B** and **T**) are twofold-degenerate, being found in two enantiomeric conformations, and consequently, each transition state is fourfold-degenerate. Along the conformational transition from one enantiomer to the other of the same conformational type, the C_{sp3}-bound hydrogens exchange their positions. The H in equatorial position in one enantiomer will be in axial position in the other and vice versa (see Figure S13 in S. I.). This phenomenon implies that the hydrogens pointing inside (H_{in}) and outside (H_{out}) the 8-member ring are continuously

exchanging their relative position during the **2-TeB**/**2-TeC** equilibrium (Scheme 2).

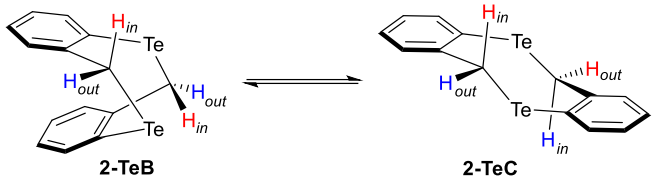

Scheme 2. Hydrogens exchange during the **2-TeB**/**2-TeC** equilibrium

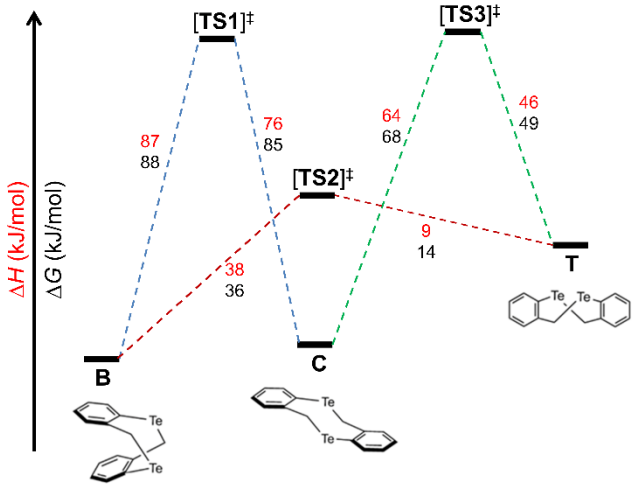

Figure 5. Gibbs free energy (black figures) and enthalpy (red figures) diagram of the conformational equilibrium of **2-Te** computed at 298K at the COSMO($CHCl_3$)-ZORA-PBE-D4(EEQ)/all electron TZP level.

Figure 5 shows the energy diagram of the conformational equilibrium in chloroform for ditellurocine **2-Te**. Conformer **B** is the most stable, being only less than 3 kJ/mol (ΔG) more stable than conformer **C** (compared to the dynamic NMR-determined ΔG of the **B**-to-**C**) conversion of ~ +5 kJ/mol), whereas conformer **T** is the least stable (ΔG(**B**→**T**) = 22 kJ/mol). The relative population of each stable conformer was calculated using Boltzmann statistics at 298 K from the Gibbs free energies computed at the COSMO($CHCl_3$, ε= 4.81)-ZORA-PBE-D4(EEQ)/all electron TZP level. Populations of 77% of **B**, 23% of **C** and only traces of **T** are obtained for **2-Te**. All conformational transition energy barriers have been found to be lower or equal to 88 kJ/mol in $CHCl_3$, supporting the hypothesis of a possible conformational exchange at room temperature. The lowest energy barrier is found for the conversion from conformer **T** to conformer **B** (ΔG(**T**→[**TS2**]‡) = 14 kJ/mol), suggesting a very fast conversion of any possibly formed **T** into **B**. The **B** to **C** activation barrier (ΔG(**B**→[**TS1**]‡) = 88 kJ/mol) is higher than the **B** to **T** one by $\Delta\Delta G$ = 52 kJ/mol. However, the **C** to **T** barrier (ΔG(**C**→[**TS3**]‡) = 68 kJ/mol) is lower than the **C** to **B** one by $\Delta\Delta G$ = 17 kJ/mol. These barriers suggest a rather fast equilibrium between **B** and **T** and much slower ones between **B** and **C** or between **C** and **T**. It is worth noting that the energy profile computed using the slightly more polar CH_2Cl_2 COSMO(CH_2Cl_2, ε= 8.93) only affects the **B**→[**TS1**] ‡ and **C**→[**TS1**]‡ barriers by lowering them by ca. 20 kJ/mol, leaving the other barriers identical and the ΔG(**B**→**C**) unchanged as compared to the COSMO($CHCl_3$) geometries. Note also that among the three transition states considered here, the singlet state geometries of [**TS1**]‡ and [**TS3**]‡ in both CH_2Cl_2 and $CHCl_3$ have the highest dipole moments of ca μ= 2 D, whereas [**TS2**]‡ exhibit a lower dipole (1.27 < μ < 1.39 D), which might suggest a strongest stabilization of the former in polar solvents. At this stage it cannot be excluded that solvent polarity change may slightly change the **B**:**C** ratio. It also must be stressed that the COSMO treatment of solvation might be insufficient for the tellurium atoms which may establish specific interactions with solvent molecules if one takes into account the law of mass action. To figure out the extent of this potential problem, the thermochemistry of the **2-TeB/2-TeC** equilibrium was computed assuming that each Te center was interacting with 1 molecule of chlorinated solvent. Both CH_2Cl_2 and $CHCl_3$ were considered. Computation indicated that explicit solvent interactions on both **2-TeB** and **2-TeC** added to the COSMO implicit solvation brings the Gibbs free energy of the **2-TeC** → **2-TeB** reaction to ΔG~ -25 kJ/mol (Figure 6) instead of the ca. -3 kJ/mol for the COSMO treatment only. If one considers the value of the Gibbs free energy for the same equilibrium determined by dynamic NMR (see Table S7 in S. I.), i.e ~-5kJ/mol, we assume that explicit solvent interaction is not significantly interfering.

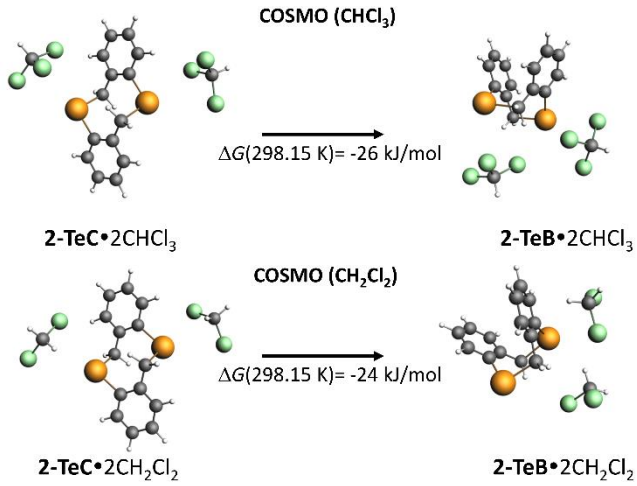

Figure 6. Thermodynamic effect of explicit solvation on the Gibbs free energy of conversion of the **2-TeC** conformer into the **2-TeB** conformer when including 1 molecule of solvent per Te centre. Atom color code: grey, C; light grey, H; light green, Cl; ochre, Te. Interatomic Te-Cl distances are comprised between 3.7 and 4.1 Å.

Qualitatively, the energy profiles computed for the two other dichalcogenocines **2-S** and **2-Se** using COSMO(CH_2Cl_2) (see Figure S14 and S15 in S.I.) are similar in features and energy barriers scale.

For **2-Te**, using the DFT free energy barriers and the resulting rate constants at 298K (obtained from transition state theory),[30] a kinetic model involving the 6 elementary reactions of Figure 5 was implemented (see Table S16 and Figure S16 in S.I for details). Starting from **B**, the numerical simulation reveals that **C** is produced after a few milliseconds and **T** is a very short-lived species. A half-life of ~ 3 ms is predicted for **B**, confirming a possible **B** to **C** interconversion at the millisecond timescale, consistent with the observed NMR results (see next section).

Geometrical data calculated for the different conformers of **2-Te** with COSMO(CH_2Cl_2) are reported in Table 1. Even though the distance between Te and the proximal H (H_{in}) on the opposite C_{sp3} (C_{12}) is shorter in the **B** and **C** conformers than in the **T** and in the transition states, no substantial variation of the C_{12}-H_{in} bond distance occurs along the conformational changes. In all conformers, the C_{12}-H_{in} is slightly longer than the C_{12}-H_{out} one ($\Delta d \leq 0.002$ Å), but not enough to be owed to a Te---H hydrogen bond. In the **B** and **C** conformers, C_{12}-H_{in} bond seems to point towards the opposite Te, while it does not in **T**. The distance between Te and H_{in} in **B** conformer is very close to the observed distance in the solid state (Figure 3) and slightly shorter than in **C** conformer (2.864 vs 2.906 Å). These values are in the range or below the reported Te---H distances in compounds where the hydrogen is bore by a carbon atom.[16,18]

Table 1. Geometric in the singlet ground states of the different conformers of **2-Te**

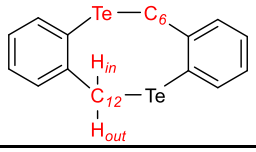

Distance (d, [Å]) or angle (α, [°])	B	C	T	[TS1]‡	[TS2]‡	[TS3]‡
d(Te-Te)	4.517	4.445	3.821	3.821	4.330	3.734
d(Te-C_6)	3.422	3.436	3.523	3.931	3.605	2.227
d(Te-H_{in})	2.864	2.906	3.523	4.467	3.319	3.470
d(Te-H_{out})	4.416	4.438	4.685	4.828	4.678	4.680
d(C_{12}-H_{in})	1.096	1.097	1.095	1.099	1.096	1.096
d(C_{12}-H_{out})	1.095	1.095	1.093	1.097	1.094	1.091
α(Te-H_{in}-C_{12})	111.6	109.8	5.0	31.2	96.3	87.3
α(C_6-Te-H_{in})	77.6	81.8	50.2	118.1	53.6	63.0

Conformational analysis by ^{1}H NMR

Theoretical conformational analysis revealed the presence of **2-TeB** and **2-TeC** as the main and minor conformers (77:23 respectively), but also the possible presence of a NCI between Te and the facing hydrogen within the ring (H_{in}) in both conformers. To validate these predictions and to obtain experimental thermodynamic and kinetic parameters, the conformational equilibrium was analyzed by NMR.

The ^{1}H NMR spectra of **2-Te** were recorded in $CDCl_3$ at different temperatures between -35°C and 25°C with an increment of 10°C (Figure 7 and S5 in S. I.). Four sets of signals corresponding to the benzylic protons are observed in all spectra indicating the presence of two conformers in solution with a ratio slightly varying with the temperature (from 89:11 to 90:10 while raising NMR temperature, see Table S7 in S. I.).

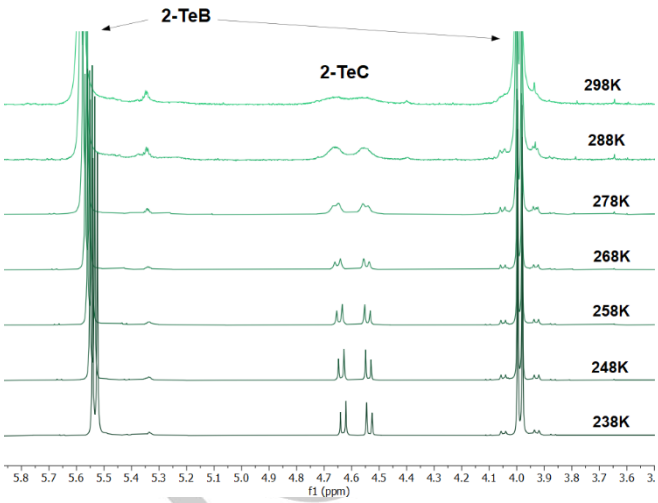

Figure 7. Variable temperature ^{1}H NMR of **2-Te** in $CDCl_3$

According to calculations of the conformational preference of **2-Te** (see previous section), the two conformers can be assigned as boat **2-TeB** (3.99 and 5.54-5.58 ppm) and chair **2-TeC** (4.54 and 4.64 ppm), respectively as the major and the minor conformers. In **2-TeB**, these hydrogens exhibited a large shift difference ($\Delta\delta$ ~ 1.57 ppm). The more shielded at 3.99 ppm showed small satellite peaks corresponding to a spin-spin coupling with ^{125}Te which could be accurately calculated at low temperature ($|^2J_{Te\text{-}H}|$ = 71.1 Hz at 238K). Although coupling with the other hydrogen (J = 9.9 Hz), the deshielded hydrogen at ~ 5.56 ppm did not exhibit clear satellite peaks. In contrast, the corresponding hydrogens in **2-TeC** appeared as an AB system (δ = 4.59 ppm, J = 10.0 Hz) without clear satellite peaks, even at low temperature. It is worth noting that the **B/C** conformational change for **2-Te** is observed at 25°C, whereas it is observed at about -20°C for **2-Se**[13] and at about -60°C for **2-S**.[8a] These results cannot be explained by the performed DFT calculations since the $\Delta G^‡$ values for the **B** to **C** transition states in **2-Te**, **2-Se** and **2-S** are in the same range (Figure 5 and Figures S14 and S15 in S. I.).

The two conformers were also observed at 298K by ^{125}Te NMR, in which they exhibit two doublets because of Te-H spin-spin coupling, one intense at 653.3 ppm corresponding to **2-TeB** ($|^2J_{Te\text{-}H}|$ = 71.1 Hz) and a small broad doublet at 633.3 ppm for **2-TeC** ($|^2J_{Te\text{-}H}|$ ~ 38.0 Hz). For the major conformer **2-TeB**, the ^{125}Te-^{1}H 2D HMQC spectrum showed two different couplings, a large one with the peak at 3.99 ppm confirming the strong Te-H spin-spin coupling ($|^2J_{Te\text{-}H}|$ = 71.1 Hz) observed in ^{1}H NMR, and a small one with the peak at 5.56 ppm ($|^2J_{Te\text{-}H}|$ = 13.8 Hz) (see Figure S4 in S. I.).

In order to confirm the conformer assignment and to distinguish between H_{in} and H_{out} (see Scheme 2), ^{1}H NMR spectra and relevant nuclear spin-spin coupling constants of **2-TeC** and **2-TeB** were computed by DFT methods using the NMR[31] and CPKS[32] subroutines of the Amsterdam Modeling Suite AMS2021.01 on geometries originally optimized at the COSMO(CH_2Cl_2)-ZORA-PBE-D4(EEQ)/all electron TZP level (see section VIII in S. I.). Relativistic effects particularly relevant with Te compounds were accounted for by scalar correction using the Zeroth Order Relativistic Approximation at the

COSMO(CH_2Cl_2)-PBE0[33] /all electron TZP level to provide a set of data comparable to those reported by Rusakova *et al*.[34] In both conformers, computations showed that proton H_{out} was shielded with respect to H_{in}. In **2-TeB**, H_{out} would show up at ca. 3.78 ppm and H_{in} at ca. 5.40 ppm. In **2-TeC**, H_{out} reduces its shielding showing up at 4.33 ppm, whereas H_{in} shows up now at 4.69 ppm. The gem $^2J_{Te\text{-}H}$ coupling constants of both protons with Te differ rather drastically with $|^2J_{Te\text{-}Hout}$ (-96 Hz)| >$|^2J_{Te\text{-}Hin}$ (-39 Hz)| in **2-TeB**. In **2-TeC** the same predominance of $^2J_{Te\text{-}Hout}$ (-84 Hz) over $^2J_{Te\text{-}Hin}$ (-33 Hz) is found. Note that the $^4J_{Te\text{-}H}$ coupling constant between the Te and the H_{in} of the opposite CH_2 moiety that is supposedly engaged in weak interaction across the ditellura 8-membered ring amounts to less than 3 Hz in absolute value in both conformers. Although the coupling constants are overestimated, these calculations confirmed the clear difference between H_{in} and H_{out} in both conformers and allowed unambiguous assignment of the two hydrogens. However, the occurrence of a Te---H_{in} bond in solution could not be clearly confirmed by the combined theoretical and experimental data.

Variable-temperature (VT) ^{1}H NMR spectra were used to calculate the Gibbs free energy ($\Delta G°$) corresponding to the equilibrium between **2-TeB** and **2-TeC** (see section V in S. I.). For each temperature, the K_{eq} value was calculated from the respective population of **2-TeB** and **2-TeC** by integration of the benzylic protons. The plot of $1/T$ against $\ln K_{eq}$ resulted in a line from which $\Delta H°$ (1.2 ± 0.1 kJ/mol) and $\Delta S°$ (-13.1 ± 0.5 $J.K^{-1}.mol^{-1}$) were determined. These values allowed to measure at 298K a $\Delta G°$ value of 5.1 ± 0.3 kJ/mol for the **2-TeB** to **2-TeC** equilibrium, in the same range as the calculated value (ΔG_{298K} = 3 kJ/mol, see Figure 5). The positive value of $\Delta G°$ is consistent with a predominance of the boat over the chair conformer at 298K.

As noticed before, during the **2-TeB**/**2-TeC** equilibrium, the benzylic protons are constantly exchanged from the "outside" to the "inside" position (see hydrogens in red and blue in the structures of **2-TeC** and **2-TeB**, Scheme 2). This interconversion was detected in the ^{1}H 2D ROESY spectrum, showing off-diagonal cross-peaks between H_{in} and H_{out} of both conformers (see Figure S2 in S. I.). By conducting EXSY experiments at four different temperatures, the rate constant (k_{obs}) could be deduced, giving access through the Eyring equation to the activation parameters associated to the conformational change between **2-TeB** and **2-TeC** (Table 2, see section VI in S. I. for details).

For $\Delta G^‡$ values, DFT calculations closely matched with the experimental values (**2-TeB** → **[TS1]‡**: 78 vs 63 kJ/mol; **2-TeC** → **[TS1]‡**: 73 vs 60 kJ/mol). Moreover, the energy difference between $\Delta G^‡$ of **2-TeB** → **[TS1]‡** and **2-TeC** → **[TS1]‡** transitions resulted in a value of 5 kJ/mol, very close to the value of $\Delta G°$ obtained from VT ^{1}H NMR experiments (5.1 kJ/mol).

Table 2. Standard entropy of activation ($\Delta S^‡$), standard enthalpy of activation ($\Delta H^‡$) and activation Gibbs free energy ($\Delta G^‡$) at 298K for the **2-TeB**/**2-TeC** interconversion.

Transition	$\Delta S^‡$ [$J.K^{-1}.mol^{-1}$]	$\Delta H^‡$ [kJ/mol]	$\Delta G^‡$ [kJ/mol]
2-TeB → **[TS1]‡**	-155 ± 8	32 ± 2	78 ± 5
2-TeC → **[TS1]‡**	-141 ± 8	31 ± 2	73 ± 5

It is worthy to stress here that solvation might have a significant role on the **2-TeB**/**2-TeC** equilibrium, which cannot satisfactorily be accounted for by theory using static continuum screening models of implicit solvation such as COSMO.[35] This issue was particularly revealed here by conducting the ^{1}H NMR analysis of **2-Te** in toluene-d_8 at 238 K, as a slight difference in the **B/C** ratio was observed, changing from 89:11 in $CDCl_3$ to 93:7 in toluene-d_8 (see Figures S5 and S6 in S. I.) and thus with a slightly different $\Delta G°$ (5.6 vs 5.1 kJ/mol) (see Table S8 and Figure S8 in SI).

QTAIM Analysis.

The quantum theory of atoms in molecule (QTAIM)[36] can address chemical bonding by the analysis of the electron density topology, which provided a preliminary insight into the interactions of the molecular systems studied therein. The joint existence of bond critical points (BCP) and bond paths (BP) can be the signature of strong to weak bonds. The QTAIM analysis of **2-TeB** and **2-TeC** (COSMO CH_2Cl_2 geometries) reveals two Te---H_{in} BP and BCP associated with rather low electron densities of around $\rho\sim$ 0.014 a.u. In comparison, the neighboring Te-C_{Ar} interactions hold stronger ρ values of 0.108 au at their BCP quite consistent with a strong two-center covalent bond (Figure 8). However, there is a limit to the QTAIM approach for diffuse multicenter interactions, which may escape a complete description that meet the expectation formalized by the VSEPR model.[37] That is the reason why a complementary IGM approach,[24] not relying on the existence of BCP, was carried out.

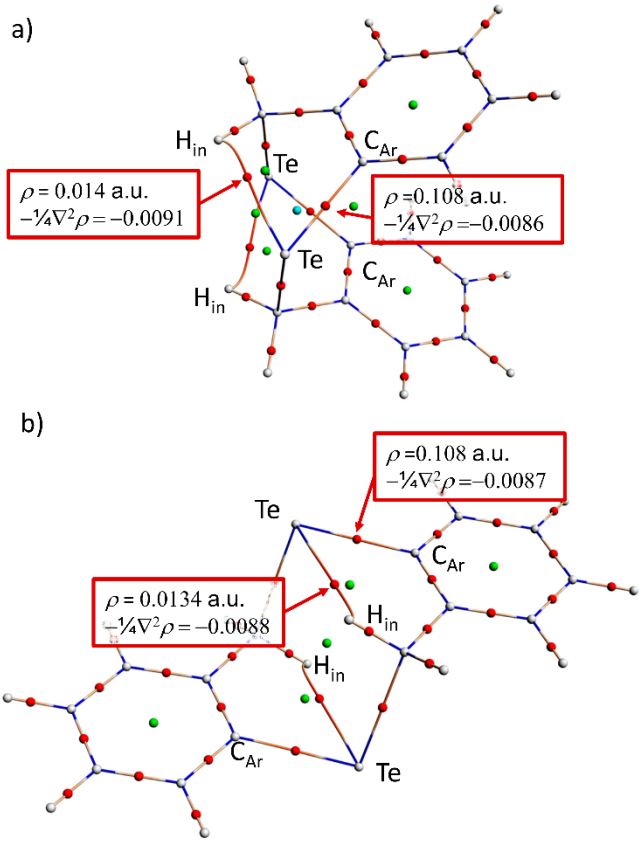

Figure 8. a) QTAIM analysis of **2-TeB**; b) QTAIM of **2-TeC**. Red dots correspond to bond critical points, green dots to ring critical points, atomic centres (light grey dots) are connected to interacting centres by bond path (coloured by density gradient scales).

IGM analysis

Following up the preliminary QTAIM analysis, an IGM investigation was undertaken in an attempt to figure out the larger stability of the boat conformer relatively to the chair-like one in isolated molecules, looking for the putative intramolecular Te---H noncovalent interaction, since one hydrogen clearly points towards the Te atom in the 8-membered ring of **2-Te**. The IGM is a recent electron density (ED) overlap-based computational method that enables to detect and quantify covalent and noncovalent chemical interactions.[24] It employs a local descriptor, δg, which quantifies the electron density clash between two given sources (atoms or fragments or molecules). In other words, δg accounts for the tendency of electrons to be shared between user's defined fragments. δg is collected for every nodes of a three-dimensional grid enclosing the system. In this study, ED was calculated from the wave function of the DFT optimized geometry and used to reveal any possible non-bonded Te---H interaction in **2-Te**. The IGM analysis operates on multiple levels of interpretation. First, the 2D plot of δg as a function of the signed ED gives a picture where one or more peaks appear, leading to a specific signature of the interaction (see Figure 9 and Figure S20 in S. I.). The larger the peak, the more intense the interaction. Here, an interaction between Te and the hydrogen atom (H_{in}, Scheme 2) of the opposite benzylic group (as shown in Figure 10 in the boat conformer) has been identified and is predicted to belong to the weak interaction family since the associated peak height δg^{peak} (0.026 a.u., in blue on Figure 9 and Figure S20 in S. I.) lies in between that of the typical hydrogen-bond in the water dimer (δg^{peak} = 0.062 a.u.) and that of the π-stacking present in the conformation of the benzene dimer (δg^{peak} = 0.012 a.u.). This benzylic hydrogen in **2-Te** is clearly involved in a NCI with the Te atom, contrary to the ipso hydrogen H_{out} exhibiting no specific NCI.

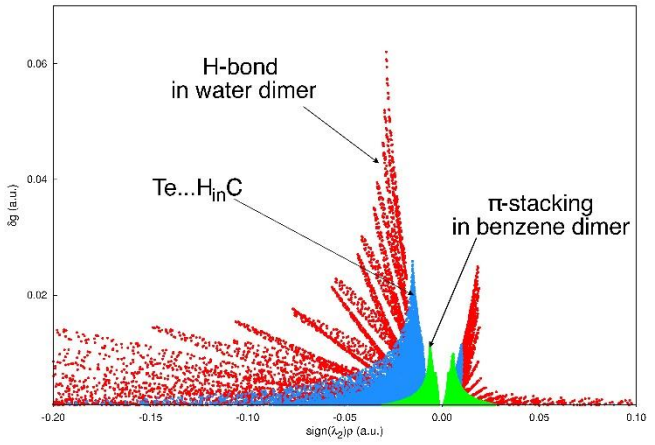

Figure 9. Te---H_{in}C interaction δg signature revealed by the IGM approach in the boat conformer of **2-Te** (blue). Hydrogen bonding in water dimer (red) and π-stacking in benzene dimer (green) are also reported for comparison.

In addition, an isosurface associated with a given δg isovalue can be generated in the real space, highlighting the spatial localization of the interaction between the interacting fragments. It can be colored on a BGR (blue-green-red) color-scale according to the signed ED. As a result, strongly or significantly attractive (e.g., covalent, hydrogen-bonds), weak (e.g., van der Waals) and non-bonding interactions are denoted by a blue, green and red color, respectively. Noteworthy, in Figure 10, the shape of the isosurface reveals that, not only the H_{in} atom but the C-H_{in} bond is actually involved in the interaction with the facing Te atom. This isosurface clearly differs from what is usually obtained for van der Waals interactions associated with flat δg isosurfaces within the IGM approach. But it is also distinct from the symmetrical disc-shaped δg isosurfaces linked with purely hydrogen-bonding. Here, although not pronounced, the δg isosurface between Te and CH_{in} is slightly elongated in the CH_{in} bond direction.

Furthermore, in order to quantitatively assess the overall strength of the interaction between the Te and CH_{in} fragments, it is necessary to resort to the IGM integration scheme of δg: $\Delta g = \int_v \delta g \, dv$ (*dv* is an elementary volume related to the grid enclosing the chemical system). Here, $\Delta g = 0.202$ a.u. is obtained for the Te---H_{in}C interaction in the boat conformer, hardly larger than $\Delta g = 0.191$ a.u. found for the analogous interaction in the chair conformer. For comparison, the hydrogen-bond in the water dimer and in the π-stacking of the benzene dimer exhibit Δg values of 0.279 a.u. and 0.412 a.u., respectively. The same conclusion (similar Ch---H_{in}C interaction in boat and chair conformers) holds across the chalcogen series S, Se, Te (see Table S21 in S. I.). Hence, we suggest that the boat conformational preference in compounds **2-S**, **2-Se** and **2-Te** cannot be ascribed to a so-called C-H---Ch hydrogen bond, as earlier stressed by some authors for species **2-Se.**[13]

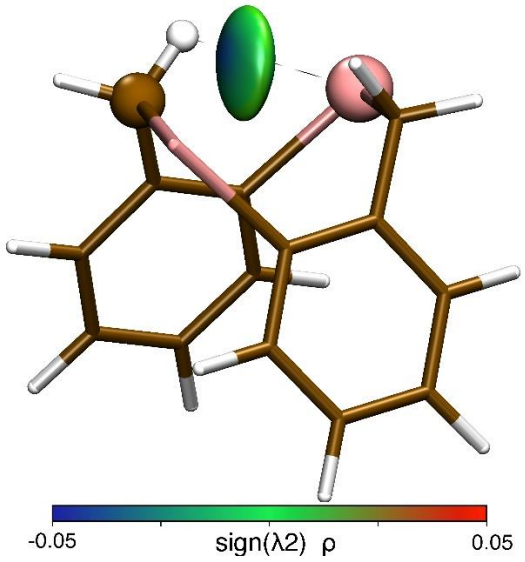

Figure 10. 0.008 δg-isosurface associated with the Te---H_{in}C interaction in the boat conformation of **2-Te**; isosurface colored according to the BGR scheme over the range -0.05 a.u. < sign(λ_2)ρ < 0.05 a.u. The CH_{in} and Te atoms involved in the interaction are rendered using the CPK representation.

To complement this investigation, we carefully examined the possible interaction between the two Te atoms. The IGM- δg interaction signature displays a peak at 0.004 a.u. for both the boat and chair conformations, one order of magnitude lower than the interaction identified between Te and H_{in}C (δg^{peak} = 0.026 a.u.). This result rules out intramolecular Te---Te interaction as the possible cause for the boat conformer preference.

Finally, the intramolecular interaction between the two phenyl rings was assessed. Actually, the π-stacking interaction is a key notion to a large part of chemist's qualitative understanding of NCIs. In intramolecular situation, this interaction is expected to play a relevant role in stabilizing certain conformations, and can even be partly responsible of specific channels within an overall reaction mechanism.[38] From this perspective, prior to any calculation, the two conformers exhibit a clear difference since only the boat conformation can significantly bring the two phenyl rings close to each other. An IGM-δg analysis was performed in an attempt to clarify and quantify this point. For the boat conformer, the obtained δg^{peak} (0.017 a.u.) points to a van der Waals interaction (see Figure S20 in S. I.). The corresponding δg isosurface is depicted in Figure 11. Owing to the poor alignment of the two interacting fragments in the boat conformation of **2-Te** (compared to the parallel-displaced benzene dimer), the resulting isosurface is not very widespread. The atomic decomposition scheme of the IGM tool[39] has been used to shed light on the interaction on a per atom basis (right panel on Figure 11). It confirms that two carbon atoms of each fragment mostly contribute (57%) to the intramolecular NCI between the two rings in the boat conformer. The resulting strength of interaction measured by the integration of δg ($\Delta g = 0.362$ a.u.) is slightly lower than the pure benzene dimer π-stacking ($\Delta g = 0.412$ a.u.), thus clearly significant. In comparison, the chair conformer shows as expected a very limited phenyl ring interaction ($\Delta g = 0.044$ a.u.). This analysis was extended to **2-S** and **2-Se** (boat and chair) with Δg gradually decreasing as we go down the chalcogen group in the boat conformation, with $\Delta g = 0.423$, 0.364 and 0.362 a.u. for S, Se and Te, respectively. Noteworthy, the intramolecular phenyl ring interaction is always given one order of magnitude larger in the boat conformation than in the chair conformation, in full agreement with the relative potential energies obtained at the COSMO(CH_2Cl_2)-PBE-D4(EEQ)/all electron TZP level of theory for isolated molecules. It should be noticed, however, that the IGM approach is based on the electron density, not taking into consideration any thermal feature nor ZPVE correction for the system.

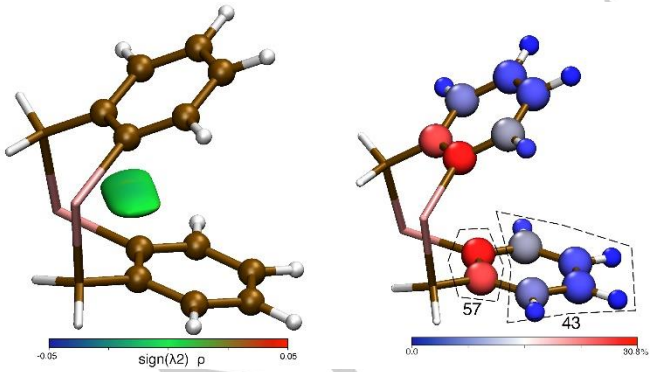

Figure 11. IGM analysis: [1, left] 0.008 δg-isosurface associated with the phenyl---phenyl interaction in **2-Te** (boat); isosurface colored according to the BGR scheme over the range -0.05 a.u. < sign(λ_2)ρ < 0.05 a.u.; the fragment atoms involved in the interaction are rendered using the CPK representation [2, right] atom colored according to Δg^{atom} (atomic contribution to the interaction in %) using a BGryR color scale, from promolecular electron density.

Beyond NCIs, we also investigated a potential C_{sp2}-Te covalent bond difference between boat and chair conformations. Actually, one Te lone pair is likely part of the adjacent phenyl ring conjugated system and one could expect the boat-chair conversion to affect this delocalized π-bonding and so by extension to affect the C_{sp2}-Te bond strength. A suitable tool to probe the bond strength between two given atoms is the IGM-IBSI index.[40] First, this analysis discloses that the C-Te bond is the most fragile bond of molecular structure **2-Te**, with IBSI values in the range 0.315-0.369, low on the IBSI scale ranging covalent interactions from 0.15 to 4.00 (with IBSI (H_2) = 1.00). Furthermore, the IGM-IBSI inspection confirms the presence of multiple bonding between C_{sp2} and Te. For instance, in the boat conformer, the intrinsic bond strength between C_{sp2} and Te is 0.364, larger than for the neighbouring single Te-C_{sp3} bond (IBSI = 0.319), as corroborated by the associated bond lengths: 2.151 and 2.229 Å, respectively. Finally, no Te-C_{sp2} bond strength difference is observed between the boat and chair conformations, discarding the π-electron delocalization between the 8-membered ring and its flanked phenyl rings as the possible cause of the boat conformational preference.

As aforementioned, **2-Te** also adopts the boat conformation in the solid state. In addition to the previously shown intramolecular interaction between phenyl rings in isolated molecule, IGM analysis achieved on the three-dimensional packing of 80 molecules of **2-Te** (based on the X-ray structure and using the promolecular ED approximation) evidences intermolecular interactions between subunits (see Figure 12). Each of the two phenyl-CH_2 groups of the central unit causes two widespread T-shaped π-stacking interactions with two distinct phenyl-CH_2 groups in neighbouring molecules. This feature is illustrated in Figure 12 for the phenyl-CH_2 group at the bottom of the central unit interacting with molecules noted ② and ③. Interestingly, intermolecular Te---Te interactions slightly contribute to these two isosurfaces. The last three isosurfaces displayed on the left of the central unit on Figure 12 correspond to a kind of phenyl---phenyl "long range sandwich interactions" involving the central molecule and adjacent subunit ①. Together, the two Te atoms contribute around 13% to the intermolecular interaction (see Figure 12). These intermolecular interactions might be completely different in a chair-like conformation. Why compound **2-Te** adopts the boat conformation in solid state, unusual for this class of molecules, rather than the chair conformation, can thus be an accumulation of various NCI. Nevertheless, it still needs further investigation, but rationalizing this observation would require exploring the potential energy surface of a very large system (several cells) at the quantum mechanics level of theory to identify a possible chair-like minimum. Then, comparing boat and chair states would shed light on intermolecular interactions dictating the conformational fate in solid state. This is clearly beyond the scope of the present study.

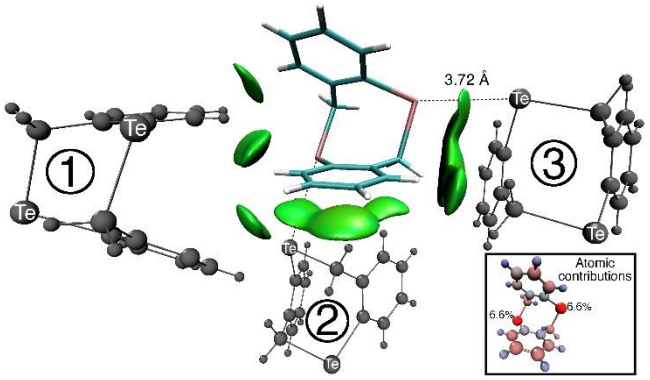

Figure 12. Main 0.006 δg-isosurfaces associated with the interaction between a central unit (rendered using the colored licorice representation) and three peripheral units ①, ② and ③ (grey) in the X-ray structure of **2-Te**; isosurface colored according to the BGR scheme over the range -0.08 a.u. < sign(λ_2)ρ < 0.08 a.u.. For the sake of clarity, half of the δg-isosurfaces has been reported (all of them can be generated through symmetry operations); atomic contributions to the interaction in the range [0%:6.6%], with atoms colored using a BGryR color scale, from promolecular electron density.

Maximum electrostatic potential (V_{max}) analysis

In the previous section, the role of intramolecular NCIs was deeply analyzed on isolated dibenzochalcogecines. However, in solution, intermolecular NCIs with surrounding solvent molecules cannot be neglected,[41] although these molecules seem relatively non-polar. Indeed, it is now well-established that chalcogens are able to participate in NCIs with nucleophilic partners through their σ-holes.[42] The resulting interaction, called chalcogen bond (ChB),[43] was shown to be involved in many applications[44] such as crystal engineering,[45] supramolecular chemistry[46] and catalysis.[47,48]

One accepted way of characterizing the anisotropy and magnitude of the electrostatic potential at halogen centres and likewise at chalcogen centres is to determine its maximum value V_{max} at localized σ-holes.[49] By convention V_{max} is determined as the value of electrostatic surface potential (ESP) at the intersection of the molecular surface defined by an electron density of 0.001 au.[50] Per se, V_{max} informs of the relative Lewis acidity of a σ-hole, which is an important information to gauge possible interactions of the chalcogen centre with its environment. ESP maxima, V_{max}, were computed using the Multiwfn program[51] for the **2** series in the **B** and **C** conformations. While two σ-holes are observed on each Te of **2-Te** in each of the two conformers, only one is observed on each Se of **2-Se** and none on each S of **2-S**. For both **B** and **C** conformers, the strongest σ-hole for **2-Te** is located facing the C_{sp2}-Te bond (V_{max} = 0.89 eV in **2-TeB** and V_{max} = 0.85 eV in **2-TeC**) and the weakest is located facing the C_{sp3}-Te bond (V_{max} = 0.31 eV in **2-TeB** and V_{max} = 0.35 eV in **2-TeC**) (see Figure S21 in S. I.). In the **2-Se** case, only the σ-hole located facing the C_{sp3}-Te bond appears accessible, while very weak (V_{max} = 0.05 eV in **2-SeB** and V_{max} = 0.09 eV in **2-SeC**).

It is interesting to note that the σ-holes in **2-Te** contribute to the formation of the Te_4 square in the solid state (see Figure 3) where the lone pair of Te atom involved in C_{sp3}-Te bond in one molecule points toward the σ-hole of Te atom involved in C_{sp2}-Te bond of another molecule. The distance of 3.724 Å between two Te atoms is far below the sum of van der Waals radii (4.12 Å), indicating a strong interaction in the solid state. Moreover, the angle of 166.5° for the C_{Ar}-Te---Te interaction is close to linearity. These geometric parameters along with the calculated Te σ-hole V_{max} values strongly support that the crystal packing of **2-Te** is mainly dominated by Te---Te ChBs.[52] These interactions may also play a role in solution depending on the nature of the solvent.

As shown in the previous sections, the difference in conformational equilibrium between the three dichalcogenocines observed experimentally in solution cannot be explained alone by the molecular data provided by DFT data dubbed with an implicit solvation model. One of the limitations of the implicit solvation approach embodied by continuum screening models such as COSMO is that, by construction, they do not account for the hardly predictable specific (explicit) interactions of the solute with the solvent. However, the presence of Te σ-holes in Te-containing molecules should induce by virtue of the law of mass action the existence of intrinsically weak but thermodynamically significant σ-hole based chalcogen-solvent interactions, particularly with halogenated or other donor solvents. Such interactions may affect the conformational equilibrium, and the relative stabilities of conformer-solvent complexes should interfere in the overall thermodynamics.[53]

Conclusion

The conformational analysis of the readily prepared ditellurocine **2-Te** was performed in solution with the aid of DFT calculations and NMR analyses. The collected data clearly show the preference for the boat conformer **2-TeB** over the chair conformer **2-TeC**. The deep NMR study in solution allowed to obtain all the thermodynamic parameters for the **2-TeB**/**2-TeC** equilibrium.

To go beyond the DFT theoretical conformational study, the IGM post-processing tool based on electron density has been implemented to investigate noncovalent and covalent interactions in compounds **2-S**, **2-Se** and **2-Te**. Interestingly, the IGM analysis reveals the presence of a NCI between the chalcogen and the opposite C-H bond. But in that case, there is no significant difference between the boat and chair conformations. No significant intramolecular interaction has been found between the two chalcogens. In contrast, the van der Waals interaction between the two phenyl rings, present in appreciable amounts, turns out to be a source of energy stabilization in the boat conformation for all compounds examined here. Furthermore, ESP analysis reveals the presence of two σ-holes on each Te of **2-Te** in each boat and chair conformers. Chalcogen bonds indeed occur in solid state and could possibly also occur in solution, where depending on the nature of the solvent, such ChB may change conformational preferences. Further works are in progress to evaluate such effects.

Experimental Section

Synthesis.

*6,12-Dihydrodibenzo[b,f][1,5]ditellurocine (**2-Te**)*. *t*-BuLi (1.7 M in pentane, 3.5 mL, 6.0 mmol) was added dropwise to 1-(fluoromethyl)-2-iodobenzene **5b** (0.67 g, 2.9 mmol) in freshly distilled tetrahydrofuran (20 mL) at -78 °C. The mixture was stirred for 1 h at -78 °C (a milky yellowish precipitate appears). Then grey tellurium powder (0.66 g, 5.1 mmol) was added in one portion, the temperature was raised to -40 °C, kept at this temperature for 40 min, then slowly raised to 0°C and stirred for 1 h. The mixture was then

quenched at 0°C by slow addition of EtOH (5 mL) and distilled water (15 mL), and further aged for 20 min at room temperature under low air flow. The mixture was filtered at vacuum over a 4 cm thick Celite pad placed in a fritted glass (porosity 1, diameter 6 cm). The pad was washed with CH_2Cl_2 (3 x 40 mL). Phases were separated and the aqueous phase was extracted with CH_2Cl_2 (40 mL). Organic extracts were combined, shortly dried over $MgSO_4$, filtered and concentrated. The crude product was purified by silica gel flash chromatography (eluent: petroleum ether / ethyl acetate, 99:1 to 95:5) to provide the desired compound. Yield 72%, 445 mg. m.p. 162-163°C, aspect: yellow solid; ^{1}H NMR – boat conformation (300 MHz, 298 K, $CDCl_3$) δ 7.40 (d, *J* = 7.3 Hz, 2H), 7.36 – 7.28 (m, 2H), 7.16 (t, *J* = 7.2 Hz, 2H), 6.62 (d, *J* = 6.9 Hz, 2H), 5.58 (d, *J* = 9.9 Hz, 2H), 3.99 (d, *J* = 9.9 Hz, 2H); ^{1}H NMR – chair conformation (600 MHz, 248 K, $CDCl_3$) δ 8.10 (d, *J* = 7.5 Hz, 2H), 7.35 – 7.32 (m, 4H), 7.25 (d, *J* = 7.5 Hz, 2H), 7.03 – 6.96 (m, 4H), 4.76 – 4.46 (m, 4H). ^{13}C{^{1}H} NMR (126 MHz, 298 K, $CDCl_3$) δ 146.8, 141.7, 130.0, 128.0, 126.0, 115.4, 14.3; ^{125}Te NMR (158 MHz, 298 K, $CDCl_3$) δ 653.3 (d, *J* = 71.1 Hz) boat conformation, 633.3 (d, *J* = 38.0 Hz) chair conformation; FT-IR (neat) 3057, 2924, 2580, 1569, 1456, 1426, 1266, 1202, 1123, 1012, 794, 750, 717, 565 cm^{-1}; HRMS (ESI–TOF) *m/z* calcd for $C_{14}H_{12}{}^{130}Te_2$: 439.9058 $[M]^+$; found, 439.9062.

Computational details.

DFT-D computations. Geometry optimization of the different conformers (minima and transition states) of **2-Te**, **2-Se** and **2-S** were performed using the SCM-ADF2019.01 package,[54] at the density functional theory (DFT) level. The Perdew-Burke-Ernzerhof (PBE) functional,[55] augmented with Grimme's fourth generation dispersion corrections with the electronegativity equilibrium model (DFT-D4(EEQ))[56] was used in all geometry optimizations. All calculations were carried out using zero-order regular approximation for relativistic effects (ZORA)[57] with an ad hoc all-electron single polarization triple-ζ Slater-type basis set (TZP).[58] Solvation was accounted for using the conductor-like screening model (COSMO)[59] assuming CH_2Cl_2 (ε = 8.9, r = 2.94 Å) as the solvent. Geometry optimizations by energy gradient minimizations were carried out in all cases with the integration grid accuracy "Normal".[60] All transition states were located using the nudged elastic band (NEB)[61] procedure. Vibrational modes were analytically computed to verify that the optimized geometries were related to energy minima or transition states.

Electrostatic surface potential analysis. Maxima of the electrostatic surface potential, V_{max}, were computed using the Multiwfn program[48] for the boat and chair conformers of **2-Te**, **2-Se** and **2-S**. The Gaussian-type wavefunctions used for these calculations were obtained from single point calculations using the Orca program package[62] version 5.0 at the ZORA-PBE-D4(EEQ) level with the def2-TZVP basis set[63] on the geometries previously optimized at the ZORA-PBE-D4(EEQ)/all electron TZP/COSMO(CH_2Cl_2) level. V_{max} were computed on an isosurface of density of ρ = 0.001 au, usually considered as the density isosurface corresponding to the van der Waals surface.

IGM calculations were performed using the code IGMplot (http://igmplot.univ-reims.fr). The interaction between chalcogen Ch (Te, Se, or S) and the opposite C-H_{in} bond (Figures 9 and 10) was investigated by defining two fragments: [Ch], [C,H], and using the wave function input file provided by DFT ZORA-PBE-D4(EEQ)/all electron TZV/COSMO(CH_2Cl_2) calculations. The intramolecular interaction between the two phenyl rings (Figure 11) and the resulting atomic decomposition analysis were addressed by defining the two C_6H_4 fragments composed of 10 atoms each. Promolecular IGM calculations were performed on a model of **2-Te** in solid state (Figure 12). First, starting from the cif input file, the Mercury program[64] was used to duplicate the unit cell in each direction, providing a lattice model of 80 molecules of **2-Te**. Next, a fragment IGM calculations was implemented, with FRAG1 = [central **2-Te** unit] and FRAG2 = [the rest of the molecules]. The VMD program[65] was employed to generate the corresponding figures. The bond strength IGM analysis was performed thanks to the IBSI index obtained by supplying the wave function input file and an atom index pair.

Acknowledgements

This research was funded by the International Center of Frontier Research in Chemistry (icFRC), the LabEx CSC (ANR-10-LABX-0026 CSC). RW thanks the LabEx CSC, Strasbourg, for a PhD fellowship. We thank the Institut de Chimie de Strasbourg (UMR 7177, CNRS-Université de Strasbourg) for a Master's 2 fellowship for LG. Thanks are given to the MaSCA (Maison de la Simulation de Champagne-Ardenne, France) and to the CRIANN computational center (Rouen, France, http://www.criann.fr) for computing facilities.

Conflict of Interest

The authors declare no conflict of interest

Keywords: chalcogen bond • conformational analysis • noncovalent interaction • σ-hole • tellurium

[1] F. Liu, H. Wang, K. N. Houk, *Curr. Org. Chem.* **2013**, *17*, 1470-1480.

[2] a) J.-H. Ha, S. N. Loh, *Chem. Eur. J.* **2012**, *18*, 7984-7999; b) G. G. Hammes, *Biochemistry* **2002**, *41*, 8221-8228.

[3] a) A. Goulet-Hanssens, F. Eisenreich, S. Hecht, *Adv. Mater.* **2020**, *32*, 1905966; b) F. Bigdeli, C. T. Lollar, A. Morsali, H.-C. Zhou, *Angew. Chem. Int. Ed.* **2020**, *59*, 46652-4669; c) S. Beyazit in *Switchable Bioelectronics* (Ed.: O. Parlak), Jenny Stanford Publishing, New York, **2020**, pp. 27-64.

[4] P. C. Knipe, S. Thompson, A. D. Hamilton, *Chem. Sci.* **2015**, *6*, 1630-1639.

[5] H. Wayment-Steele, M. Wu, M. Gotrik, R. Das, *Methods in Enzymology* **2019**, *623*, 417-450.

[6] B. A. F. Le Bailly, J. Clayden, *Chem. Commun.* **2016**, *52*, 4852-4863.

[7] a) K. W. Plaxco, H. T. Soh, *Trends Biotech.* **2011**, *29*, 1-5; b) E. J. Lemieux, M. Leclerc in *Conjugated Polyelectrolytes* (Eds.: B. Liu, G. C. Bazan), Wiley-VCH, Weinheim, **2013**, pp. 231-261.

[8] a) R. Crossley, A. P. Downing, M. Nogradi., A. Braga de Oliveira, W. D. Ollis, I. O. Sutherland, *J. C. S. Perkin 1* **1973**, 205-217; b) D. Montecalvo, M. St-Jacques, R. Wasylishen, *J. Am. Chem. Soc.* **1973**, *95*, 2023-2024; c) W. D. Ollis, J. E. Stoddart, I. O. Sutherland, *Tetrahedron* **1974**, *30*, 1903-1924; d) M. L. Jimeno, I. Alkorta, J. Elguero, J. E. Anderson, R. M. Claramunt, J. L. Lavandera, *New J. Chem.* **1998**, 1079-1083; e) I. Alkorta, J. Elguero, *Struct. Chem.* **2010**, *21*, 885-891.

[9] a) J. Elguero, A. R. Katritzky, B. S. El-Osta, R. L. Harlow, S. H. Simonsen, *J. Chem. Soc. Perkin Trans. 1*, **1976**, 312-315; b) C. Foces-Foces, F. H. Cano, P. Cabildo, R. M. Claramunt, J. Elguero, *Acta Crystallogr. Sect. C* **1991**, *47*, 2583-2585; c) P. Domiano, P. Cozzini, R. M. Claramunt, J. L. Lavandera, D. Sanz, J. Elguero, *J. Chem. Soc. Perkin Trans. 2* **1992**, 1609-1620; d) P. Cabildo, R. M. Claramunt, P. Cornago, J. L. Lavandera, D. Sanz, N. Jagerovic, M. L. Jimeno, J. Elguero, I. Gilles, J. L. Aubagnac, *J. Chem. Soc. Perkin Trans. 2* **1996**, 701-711; e) L. Kobryn, W. P. Henry, F. R. Fronczek, R. Sygula, *Tetrahedron Lett.* **2009**, *50*, 7124-7127.

[10] R. M. Claramunt, J. L. Lavandera, D. Sanz, J. Elguero, M. L. Jimeno, *Tetrahedron* **1998**, *54*, 9569-9580.

[11] W. Fu, T. M. Alam, J. Li, J. Bustamante, T. Lien, R. W. Adams, S. J. Teat, B. J. Stokes, W. Yang, Y. Liu, J. Q. Lu, *J. Am. Chem. Soc.* **2020**, *142*, 16651-16660.

[12] F. Ishiwari, S. Miyake, K. Inoue, K. Hirose, T. Fukushima, A. Saeki, *Asian J. Org. Chem.* **2021**, *10*, 1377-1381.

[13] a) M. Iwaoka, M. Tomoda, *J. Am. Chem. Soc.* **1994**, *116*, 4463-4464; b) M. Iwaoka, H. Komatsu, M. Tomoda, *Bull. Chem. Soc. Jpn.* **1996**, *69*, 1825-1828.

[14] T. Chivers, R. S. Laitinen, *Chem. Soc. Rev.* **2015**, *44*, 1725-1739.

[15] A. Chand, H. S. Biswal, *J. Indian Inst. Sci.* **2020**, *100*, 77-100.
[16] For C–H---Te interaction, see: a) T. Steiner, *J. Mol. Struct.* **1998**, *447*, 39-42; b) M. J. Poropudas, J. M. Rautiainen, R. Oilunkaniemi, R. S. Laitinen, *Dalton Trans.* **2016**, *45*, 17206-17215.
[17] For Ne–H---Te interaction, see: a) C. J. Warren, D. M. Ho, R. C. Haushalter, A. B. Bocarsly, *J. Chem. Soc. Chem. Commun.* **1994**, *3*, 361-363; b) R. Chen, J. Zhou, X. Liu, F. Hu, L. An, Y. Kan, C. Xue, *Inorg. Chem. Commun.* **2013**, *28*, 55-59.
[18] M. Ghosh, P. Panwaria, S. Tothadi, A. Das, S. Khan, *Inorg. Chem.* **2020**, *59*, 17811-17821.
[19] T. L. Hill, *J. Chem. Phys.* **1948**, *16,* 399-404.
[20] a) B. Jeziorski, R. Moszynski, K. Szalewicz, *Chem. Rev.* **1994**, *94,* 1887-1930; b) K. Szalewicz, *WIREs Comput. Mol. Sci.* **2012**, *2,* 254-272.
[21] a) K. Morokuma, *J. Chem. Phys.* **1971**, *55,* 1236-1244; b) M. J. S. Philipps, T. Fox, C. S. Tautermann, C.-K. Skylaris, *Chem. Soc. Rev.* **2015**, *44,* 3177-3211.
[22] a) R. M. Parrish, J. F. Gonthier, C. Corminboeuf, D. Sherrill, *J. Chem. Phys.* **2015**, *143,* 051103; b) P. Su, Z. Chen, W. Wu, *Chem. Phys. Lett.* **2015**, *635,* 250-256.
[23] M. A. Blanco, A. M. Pendas, E. Francisco, *J. Chem. Theory Comput.* **2005**, *1,* 1096-109.
[24] a) C. Lefebvre, G. Rubez, H. Khartabil, J.-C. Boisson, J. Contreras-Garcia, E. Hénon, *Phys. Chem. Chem. Phys*. **2017**, *19*, 17928-17936; b) C. Lefebvre, H. Khartabil, J.-C. Boisson, J. Contreras-Garcia, J.-P. Piquemal, E. Hénon, *Chem. Phys. Chem.* **2018**, *19*, 724-735.
[25] a) W. J. M. van Tilborg, R. Plomp, *Recl. Trav. Chim. Pays-Bas* **1977**, *96*, 282-286; b) E. Voigt, H. Meier, *Angew. Chem. Int. Ed.* **1976**, *15*, 117; *Angew. Chem.* **1976**, *88*, 94; c) K. Kanakarajan, H. Meier, *J. Org. Chem.* **1983**, *48*, 881-883; d) H. Meier, *J. Prakt. Chem.* **1996**, *338*, 383-385.
[26] S. Yamazaki, K. Kohgami, M. Okazaki, S. Yamabe, T. Arai, *J. Org. Chem.* **1989**, *54*, 240-243.
[27] D. Shanks, H. Frisell, H. Ottosson, L. Engman, *Org. Biomol. Chem.* **2006**, *4*, 846-852.
[28] R. Gleiter, G. Haberhauer, D. B. Werz, F. Rominger, C. Bleiholder, *Chem. Rev.* **2018**, *118*, 2010-2041.
[29] a) C. Y. Legault, CYLview, 1.0b; University of Sherbrooke, 2009 (http://www.cylview.org); b) Deposition number CCDC 2108623 (for **2-Te**) contain the supplementary crystallographic data for this paper. These data are provided free of charge by The Cambridge Crystallographic Data Centre and Fachinformationszentrum Karlsruhe Access Structures service www.ccdc.cam.ac.uk/structures.
[30] a) H. Eyring, *Chem. Rev.* **1935**, *17*, 65-77; b) D. G. Truhlar, B. C. Garrett, S. J. Klippenstein, *J. Phys. Chem.* **1996**, *100*, 12771-12800.
[31] a) S. K. Wolff, T. Ziegler, E. van Lenthe, E. J. Baerends, *J. Chem. Phys.* **1999**, *110*, 7689-7698; b) J. Autschbach, S. Zheng, *Annual Reports on NMR Spectroscopy* **2009**, *67*, 1-95.
[32] J. Autschbach, T. Ziegler, *J. Chem. Phys.* **2000**, *113*, 936-947.
[33] M. Ernzerhof, G. Scuseria, *J. Chem. Phys.* **1999**, *110*, 5029-5036.
[34] I. L. Rusakova, L. B. Krivdin, *Mendeleev Commun.* **2018**, *28*, 1-13.
[35] M. R. Milovanović, M. Boucher, Y. Cornaton, S. D. Zarić, M. Pfeffer, J. Djukic, *Eur. J. Inorg. Chem.* **2021**, 10.1002/ejic.202100750.
[36] R. F. W. Bader, In Atoms in Molecules: A Quantum Theory; Clarendon: Oxford, 1990.
[37] a) L. J. Farrugia, C. Evans, D. Lentz, M. Roemer, *J. Am. Chem. Soc.* **2009**, *131*, 1251-1268; b) M. Hamdaoui, C. Desrousseaux, H. Habbita, J.-P. Djukic, *Organometallics* **2017**, *36*, 4864-4882.
[38] H. Khartabil, L. Doudet, I. Allart-Simon, M. Ponce-Vargas, S. Gérard, E. Hénon, *Org. Biomol. Chem.* **2020**, *18*, 6840-6848.
[39] M. Ponce-Vargas, C. Lefebvre, J.-C. Boisson, E. Hénon, *J. Chem. Info. Model* **2020**, *60,* 268-278.
[40] J. Klein, H. Khartabil, J.-C. Boisson, J. Contreras-Garcia, J.-P. Piquemal, E. Hénon, *J. Phys. Chem. A* **2020**, *124,* 1850-1860.
[41] F. Würthner, *J. Org. Chem.* **2021**, 1021/acs.joc.1c00625.
[42] J. S. Murray, P. Lane, T. Clark, P. Politzer, *J. Mol. Model.* **2007**, *13*, 1033-1038.
[43] C. B. Aakeroy, D. L. Bryce, G. R. Desiraju, A. Frontera, A. C. Legon, F. Nicotra, K. Rissanen, S. Scheiner, G. Terraneo, P. Metrangolo, G. Resnati, *Pure Appl. Chem.* **2019**, *91*, 1889-1892.
[44] a) K. T. Mahmudov, M. N. Kopylovich, M. F. C. Guedes da Silva, A. J. L. Pombeiro, *Dalton Trans.* **2017**, *46*, 10121-10138; b) L. Vogel, P. Wonner, S. M. Huber, *Angew. Chem. Int. Ed.* **2019**, *58*, 1880–1891; c) N. Biot, D. Bonifazi, *Coord. Chem. Rev.* **2020**, *413*, 213243.
[45] P. Scilabra, G. Terraneo, G. Resnati, *Acc. Chem. Res.* **2019**, *52*, 1313-1324.
[46] J. Y. C. Lim, P. D. Beer, *Chem* **2018**, *4*, 731-783.
[47] a) J. Bamberger, F. Ostler, O. García Mancheño, *ChemCatChem* **2019**, *11*, 5198-5211; b) M. Breugst, J. J. Koenig, *Eur. J. Org. Chem.* **2020**, 5473-5487.
[48] For recent examples from our group, see: a) R. Weiss, E. Aubert, P. Peluso, S. Cossu, P. Pale, V. Mamane, *Molecules* **2019**, *24*, 4484; b) R. Weiss, E. Aubert, P. Pale, V. Mamane, *Angew. Chem. Int. Ed.* **2021**, *60*, 19281-19286.
[49] M. H. Kolář, P. Hobza, *Chem. Rev.* **2016**, *116*, 5155-5187.
[50] T. Brinck, J. S. Murray, P. Politzer, *Int. J. Quantum Chem.* **1992**, *44*, 57-64.
[51] L. Tian, F. Chen, *J. Comput. Chem.* **2012**, *33*, 580-592.
[52] a) S. Kolb, G. A. Oliver, D. B. Werz, *Angew. Chem. Int. Ed.* **2020**, *59*, 22306-22310; b) M. Rodewald, J. M. Rautiainen, T. Niksch, H. Görls, R. Oilunkaniemi, W. Weigand, R. S. Laitinen, *Chem. Eur. J.* **2020**, *26*, 13806-13818.
[53] M. R. Milovanović, Q. Dherbassy, J. Wencel-Delord, F. Colobert, S. D. Zarić, J.-P. Djukic, *ChemPhysChem* **2020**, *21*, 2136-2142.
[54] G. Te Velde, F. M. Bickelhaupt, E. J. Baerends, C. Fonseca Guerra, S. J. A. van Gisbergen, J. G. Snijders, T. Ziegler, *J. Comput. Chem.* **2001**, *22*, 931-967.
[55] J. P. Perdew, K. Burke, M. Ernzerhof, *Phys. Rev. Lett.* **1996**, *77*, 3865-3868.
[56] E. Caldeweyher, S. Ehlert, A. Hansen, H. Neugebauer, S. Spicher, C. Bannwarth, S. Grimme, *J. Chem. Phys.* **2019**, *150*, 154122.
[57] E. Van Lenthe, J. G. Snijder, E. J. Baerends, *J. Chem. Phys.* **1996**, *105*, 6505-6516.
[58] a) E. van Lenthe, E. J. Baerends, J. G. Snijders, *J. Chem. Phys.* **1993**, *99*, 4597-4610; b) E. van Lenthe, E. J. Baerends, J. G. Snijders, *J. Chem. Phys.* **1994**, *101*, 9783-9792; c) E. van Lenthe, A. Ehlers, E. J. Baerends, *J. Chem. Phys.* **1999**, *110*, 8943-8953.
[59] a) A. Klamt, G. Schüürmann, *J. chem. Soc. Perkin Trans. 2* **1993**, 799-805; b) A. Klamt, *J. Phys. Chem.* **1995**, *99*, 2224-2235; c) A. Klamt, V. Jonas, J. *Chem. Phys.* **1996**, *105*, 9972-9981.
[60] M. Franchini, P. H. T. Philipsen, L. Visscher, *J. Comput. Chem.* **2013**, *34*, 1819-1827.
[61] G. Henkelman, B. P. Uberuaga, H. Jonsson, *J. Chem. Phys.* **2000**, *113*, 9901-9904.
[62] F. Neese, *WIREs Comput. Mol. Sci.* **2012**, *2*, 73-78.
[63] F. Weigend, R. Ahlrichs, *Phys. Chem. Chem. Phys.* **2005**, *7*, 3297-3305.
[64] C. F. Macrae, I. Sovago, S. J. Cottrell, P. T. A. Galek, P. McCabe, E. Pidcock, M. Platings, G. P. Shields, J. S. Stevens, M. Towler, P. A. Wood, *J. Appl. Cryst.* **2020**, *53*, 226-235.
[65] W. Humphrey, A. Dalke, K. Schulten, *J. Mol. Graph.* **1996**, *14*, 33-38.

Entry for the Table of Contents

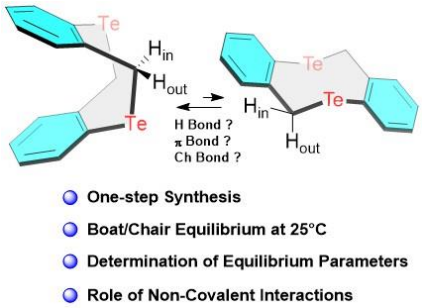

Insertion of tellurium atoms in the dibenzocyclooctadiene framework induced higher stability of the boat conformer, with an activation energy for the boat to chair conformational change of 78 kJ/mol. Besides the more stabilizing π-π stacking interactions between the benzene rings in the boat conformation, other noncovalent interactions such as chalcogen bonds with the surrounding solvent molecules might explain the observed results.

Institute and/or researcher Twitter usernames: @mamane_victor